This document is confidential and is proprietary to the American Chemical Society and its authors. Do not copy or disclose without written permission. If you have received this item in error, notify the sender and delete all copies.

Staggered fibrils and damageable interfaces lead concurrently and independently to hysteretic energy absorption and inhomogeneous strain fields in cyclically loaded antler bone

Journal:	*ACS Biomaterials Science & Engineering*
Manuscript ID	ab-2016-00637q.R1
Manuscript Type:	Article
Date Submitted by the Author:	n/a
Complete List of Authors:	De Falco, Paolino; Queen Mary University of London, School of Engineering and Materials Science Barbieri, Ettore; Queen Mary University of London, School of Engineering and Materials Science Pugno, Nicola; Università di Trento, Department of Civil, Environmental and Mechanical Engineering; Queen Mary, University of London, School of Engineering and Materials Science; Fondazione Bruno Kessler, Center for Materials and Microsystems Gupta, Himadri; Queen Mary University of London, School of Engineering and Materials Science

SCHOLARONE™
Manuscripts

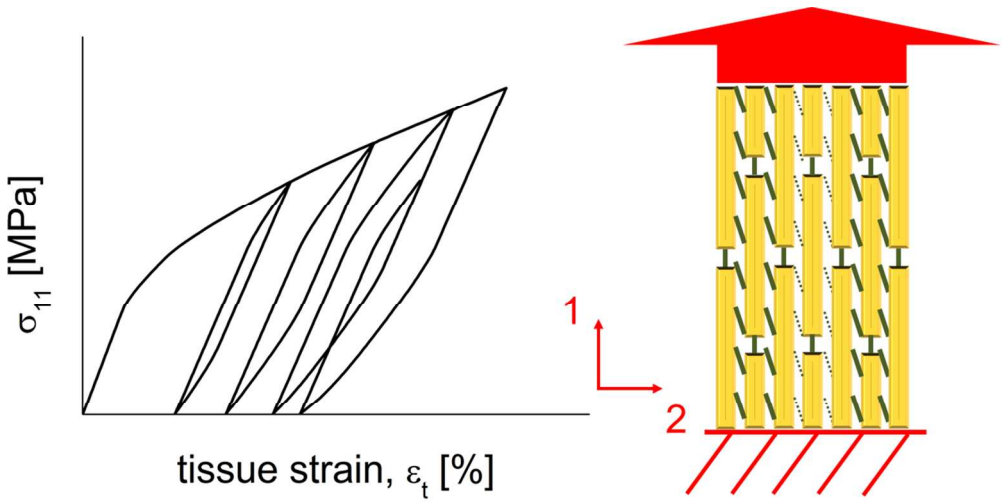

Hysteresis at the fibrillar level in the mineralized fibrils of antler bone (left) is enabled via the staggered architecture and interfaces which can fail above critical loads (right)

334x165mm (96 x 96 DPI)

Staggered fibrils and damageable interfaces lead concurrently and independently to hysteretic energy absorption and inhomogeneous strain fields in cyclically loaded antler bone

P. De Falco[a], E. Barbieri[a], N. Pugno[a,b,c] and H. S. Gupta[a*]

[a] *Queen Mary University of London, School of Engineering and Material Science, London, E1 4NS, UK*

[b] *Laboratory of Bio-Inspired and Graphene Nanomechanics, Department of Civil, Environmental and Mechanical Engineering, University of Trento, Trento, Italy*

[c] *Center for Materials and Microsystems, Fondazione Bruno Kessler, Povo (Trento), Italy*

[*] Corresponding author: Himadri S. Gupta (h.gupta@qmul.ac.uk)

Keywords

Antler bone, interface, nanoscale, cohesive behaviors, heterogeneity, hysteresis

Abstract

The high toughness and work to fracture of hierarchical composites, like antler bone, involve structural mechanisms at the molecular, nano- and micro scales, which are not completely explored. A key characteristic of the high energy absorption of such materials is the large hysteresis during cyclic loading, but its origin remains unknown. *In situ* synchrotron X-ray diffraction tests during tensile loading of antler bone showed heterogeneous fibrillar deformation and hysteresis. To explain the origin of these mechanisms from the nanostructure of antler bone, here we develop a class of finite-element fibril models whose predictions are compared to experimental data across a range of potential composite architectures. We demonstrate that the key structural motif enabling a match to experimental data is an axially staggered arrangement of stiff mineralized collagen fibrils coupled with weak, damageable interfibrillar interfaces.

1 INTRODUCTION

Natural structural materials exhibit mechanical properties through complex hierarchical architectures and load-absorbing mechanisms. These architectures evolved naturally from basic building blocks thanks to a 'self-organization' strategy during growth[1]. In fact, biological structures adapt, change function during growth, renew their material and build hierarchies[2]. The macroscopic behaviour of these materials depends on the interaction

between structural properties at different scales[3]. Bio-composites, such as bone, shells and nacre, represent an excellent example of how the design at lower hierarchical scales confers higher mechanical properties than the single constituents[4]. Although the stiffness of these biocomposites is comparable to that of the basic constituent at the nanoscale, their toughness results hugely increased. For instance, in bone and shell, the toughness of the mineral constituents is << 1MPa*$m^{1/2}$ while the toughness of their macrostructure varies, respectively, in a range of 2 - 7 MPa*$m^{1/2}$ and 3 - 7 MPa*$m^{1/2}$.

Bone, as shown in **Figure 1**, at the nanometre scale length is a composite of stiff inorganic hydroxyapatite platelets interleaved with a softer organic matrix, made principally of type I tropocollagen proteins[5]. This sub-structure, together with an intrafibrillar phase of noncollageneous proteins and mineral, forms mineralized fibrils that are arranged into aggregate structures at higher levels and larger length scales, such as fibril arrays and lamellae[1]. The structural aspects of this architecture served as inspiration for bioinspired materials that replicate the nanometre scale fibril-matrix[6-10] and intrafibrillar[11] structure, or at micrometre scales[12,13]. Nonetheless, the mechanical interactions between the constituent units and the higher length scales remain a matter of active research. In particular, previous studies focused on how the hierarchical architecture brings functionally desirable properties such as high toughness[14], energy absorption and fatigue resistance[15].

At the range of 1 – 100 μm, accepted and validated toughness mechanisms are crack deflection and bridging[16], and constrained microcracking[17]. The nanoscale structure is believed to be of fundamental importance for bone toughness. However, it is both challenging to investigate experimentally[18] as well as to explain the reasons of its mechanical properties at this scale with a model. Works to date mainly focused on either deformation beyond the yield point under uniaxial or localized loading[18-20] or on post-hoc

interpretation of electron microscopic images of loaded and fractured bone[21-22]. These experimental studies led to hypothesise different toughness mechanisms[23]. Examples include intrafibrillar plasticity[20], sacrificial bonds within noncollageneous proteins[22], friction between collagen and mineral[24], fibrillar sliding of mineralized collagen fibrils[25], interfibrillar sliding of collagen fiber arrays[26] and microcracking[27]. At these small length scales relatively less clear evidence exists on the response to cyclic loading, although recent experimental work has begun to shed light on this question. For example, Schwiedrzik et al.[28] focused on compression and cyclic micro-pillar tests on lamellar bone and measured axial and transverse apparent moduli and compressive strengths.

Bone is physiologically subjected to external periodic loading that can lead to fatigue failure, and high rate impact that instead can lead to fracture. It is then of considerable interest to understand how the nanostructure behaves under these loading conditions. Unfortunately, experimental information on the structural changes at the fibrillar and interfibrillar level in these loading modes is relatively scarce. Concurrently, the link between the types of fibrillar architecture and the developed cyclic inelastic response is also not very clear. In this regard, a recurrent generic motif in the architecture of hard biological composites is a staggered arrangement of fibrils (**Figure 2b**)[29]. This particular arrangement plays a key role in energy dissipation through sliding[30-31] and in enhancing the structural elastic properties[32-33]. Gupta et al.[20] identified elastoplastic behaviour for the individual mineralized fibril under the assumption of staggered configuration of mineral platelets and collagen molecules inside the fibril.

The role of such a staggered configuration in cyclic loading and energy absorption is unexplored at the nanoscale. Recent *in situ* synchrotron SAXD/WAXD mechanical loading/unloading tests on antler bone[20] show hysteresis in stress-strain curves at both the

macroscopic and the fibrillar level. These results also highlight the presence of two groups of fibrils: plastically deforming fibrils, which exhibit larger deformation (which will be denoted type A in what follows), and elastically deforming fibrils (denoted type B), whose deformation remains at or under the strain at the material yield point. It is clear that these structural mechanisms may be related, and that the fibrillar hysteresis is an important component of the high work to fracture of antler, but its structural origins are far less understood. *In situ* experimental probes of the type described above need to be combined with ultrastructural modelling at the scale of 1-100 nm, in order to develop a deeper understanding of the relevant mechanisms.

In this paper, we present a set of finite element simulations of the mineralized fibrils in antler bone under cyclic loading whose results, when matched to experiment, give an understanding of the causes of the fibrillar hysteresis. We will show that the combination of a damageable interface and staggered fibrillar arrangement turns out to be capable of explaining the experimentally observed hysteretic loops in loading/unloading curves. In addition, a clear explanation of the biphasic fibrillar deformation mechanisms, in terms of the dependence on interfacial strength and architecture, is here reported. These results provide new insights of toughening mechanisms at the nanoscale in antler bone.

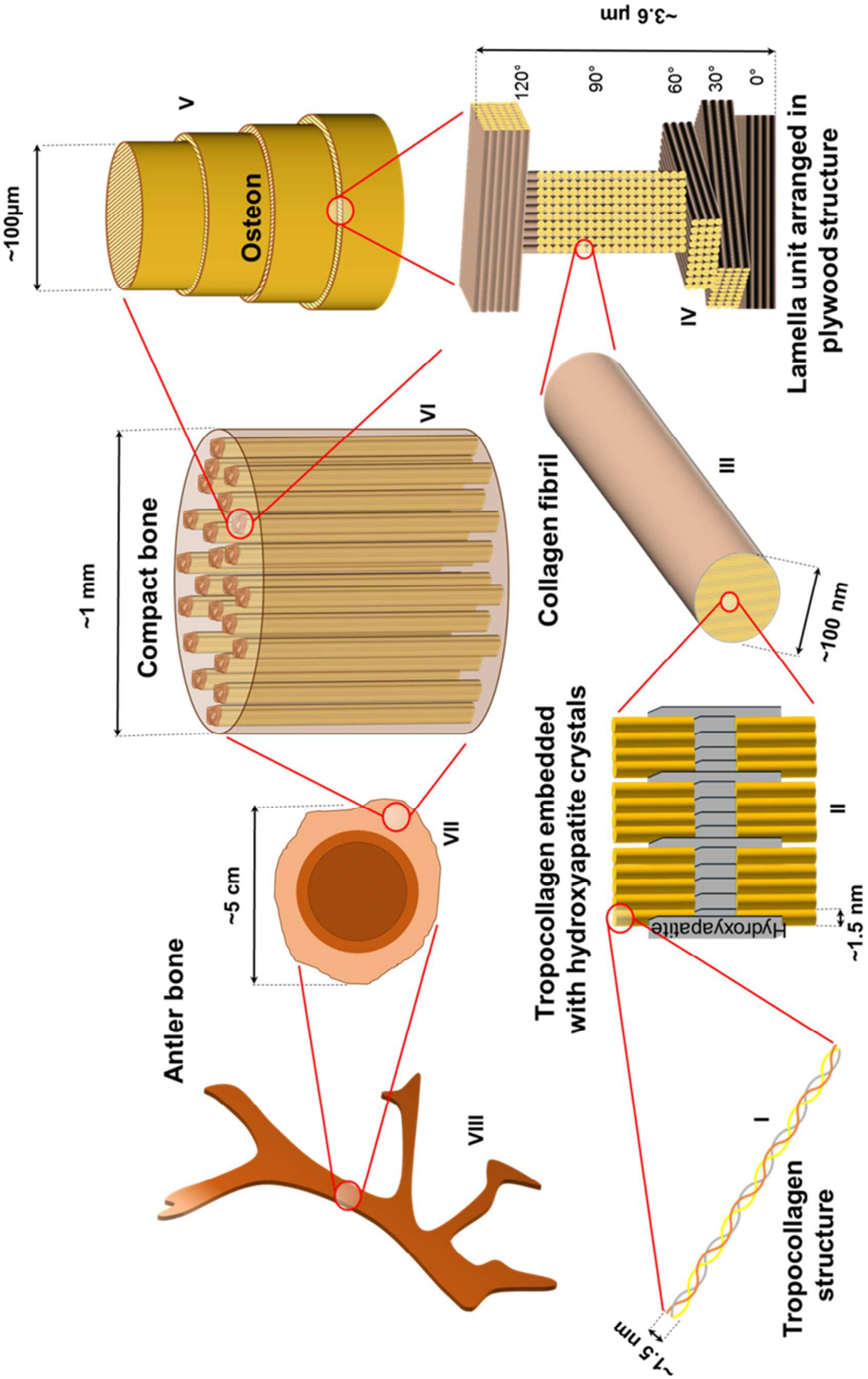
~3.6 μm
120°
90°
60°
30°
0°
V
~100μm
Osteon
IV
Lamella unit arranged in plywood structure
VI
~1 mm
Compact bone
III
Collagen fibril
~100 nm
Tropocollagen embedded with hydroxyapatite crystals
II
Hydroxyapatite
~1.5 nm
~5 cm
VII
Antler bone
VIII
I
~1.5 nm
Tropocollagen structure

99

Figure 1 - Hierarchical structure in antler bone: *The collagen fibrils (II) are made of tropocollagen molecule (I) and hydroxyapatite mineral. At the following hierarchical level, these fibrils are wrapped in a protein-based matrix (III) forming a plywood structure: the lamella unit (IV). This group is repeated in the osteon (V) which is part of the compact bone (VI) and therefore of the antler bone structure (VII-VIII).*

2 METHODS

2.1 Experimental method

The preparation description of antler bone specimens and the *in situ* mechanical tests with synchrotron small angle X-ray diffraction (SAXD) are described in detail in a previous paper[20], and summarized here briefly. The samples were taken from the antler cortical shell of a red deer (*Cervus elaphus*) near the antler-pedicle junction and tested with SAXD measurements, combined with cyclic loading. While the details are available in our previous papers [34], they will be summarized here for completeness. **Figure 2a** shows a highly simplified schematic for tensile cyclic tests on hydrated antler bone specimens combined with time-resolved synchrotron SAXD measurements, where a synchrotron X-ray beam impinges on the specimen, leading to a sequence of SAXD patterns acquired as the sample is deformed.

Meridional peaks are visible in the SAXD pattern, due to the periodic electron density profile arising from the axial D-stagger of the tropocollagen molecules inside the fibril (D~65-67 nm for vertebrate collagenous tissues). Percentage shifts in these peak positions are therefore measures of fibril strain, as reported previously for bone (e.g. Gupta et al.[35] , Dong et al.[36], Zimmermann et al.[37],among others). The 3rd order meridional peak was used

for determination of mean fibril strain, via the relation $D = 6\pi/q_{03}$ where q_{03} was the peak position, in reciprocal space, of the meridional peak. Further, the peak width w_q was also determined, which (as reported in Krauss et al.[34] and Gupta et al.[20]) provides a measure of the heterogeneity of fibrillar deformation: a narrow w_q corresponds to a uniform fibrillar deformation with all fibrils in the scattering volume deforming similarly, while an increasing w_q corresponds to an increasing heterogeneity, or dispersion, in the fibril strain distribution. As the details are presented in Gupta et al.[20], we note only that by tracking the stress-induced increase in mean fibril strain, together with the increase in w_q, a biphasic fibrillar deformation was observed, and will serve as part of the comparison of our presented model to experiment.

2.2 Numerical method and implementation of the model

Parametric finite elements simulations were performed to test a seven-layer staggered fibrillar system using Abaqus (Abaqus 6.14-1, Dassault Systemes). The two-dimensional model is made of 2800 CPS4R finite elements (CPS4R corresponds to 4-node, reduced integration with hourglass control). The plates, measuring 10 μm × 0.2 μm, represent the fibrils (with 200 nm or 0.2 μm radius[2]) in bone and are connected through cohesive laws, which are shown in detail in **Figure 2b**[38]. Interfaces link both the lateral sides of fibrils ('mode I interface') and their bottom-up sides ('mode II interfaces') (see **Figure 3c** for interfaces definition). The model (**Figure 2b**) assumes initially linear elastic behaviour (**Equation 1**, next page) followed by the initiation and evolution of damage. In **Equation 1**, the traction stress vector consists, as our models are two-dimensional, of two components t_n and t_s, which are, respectively, the normal and shear tractions, and δ_n and δ_s which represent the relative displacements between the nodes on the adjacent surfaces of two different fibrils. We decided to use the simplest traction-separation law, where normal (K_{nn}) and tangential (K_{ss}) stiffness are not coupled (K_{ns} and K_{sn} are null in **Equation 1**).

$$t = \begin{bmatrix} t_n \\ t_s \end{bmatrix} = \begin{bmatrix} K_{nn} & 0 \\ 0 & K_{ss} \end{bmatrix} \begin{bmatrix} \delta_n \\ \delta_s \end{bmatrix} \quad (1)$$

As peak traction values for the mode I and mode II undamageable interfaces, we used generic values such as $t_n^0 = t_s^0 = 80$ MPa. These values are never achieved among the finite elements adjacent to the interfaces and do not affect the results. For mode II damageable interfaces we adopted the values $t_n^0 = 80$ MPa and $t_s^0 = 0.8$ MPa; t_n^0 is an arbitrary high value, never reached upon the structure, while t_s^0 is the shear stress occurring when at least one point in the structure reaches yielding. We followed the hypothesis[20] that heterogeneity, due to progressive mode II interface damage, starts occurring in correspondence of the yielding point. We imposed this condition by choosing as shear traction peak value, the maximum shear stress, recorded in a generic point of structure, which occurs when at least one finite element reaches the yielding stress prescribed by the material model used for the simulations ($\sigma_y \approx 46$ MPa, which is the yield point observed experimentally for antler bone in Gupta et al.[20]). The damage initiation values t_n^0 and t_s^0 were chosen such that mode I interfaces are never damageable, while the mode II interfaces could be either damageable or not. Therefore, we adopted a maximum stress criterion for the onset of damage (**Equation 2**) where damage initiates when the maximum ratio between the traction values at the interface ($\langle t_n \rangle$, t_s) and the peak values (t_n^0 and t_s^0) reaches the value of one. The symbols <> represent the Macaulay brackets that are used to mean that a compressive traction does not initiate the damage.

$$max\left\{\frac{\langle t_n \rangle}{t_n^0}, \frac{t_s}{t_s^0}\right\} = 1 \quad (2)$$

We used, the values K_{nn} = K_{ss} = 100 MPa as stiffness coefficients for both mode I and mode II interfaces. The choice of K_{nn} for the mode II interface and K_{ss} for the mode I interface has no effect on the results. The response of the system was then expected to be mainly affected by K_{nn} for the mode I interface and by K_{ss} for the mode II one. We performed parametric simulations, keeping all the parameters fixed except for K_{nn} for the mode I interface and K_{ss} for the mode II interface. We varied these values between 100 and 300 MPa/μm, with a step of 100 MPa/μm (in total 9 simulations), and we found that when K_{nn} = K_{ss} = 100 MPa/μm the numerical maximum tissue strain matches the correspondent experimental value closely. We chose these coefficients such that both the numerical and the experimental systems achieve the same level of maximum tissue strain. We expressed the coefficients K_{nn} and K_{ss} as K in **Figure 2b**, as the figure is representative of a generic mode of fracture. The choice of K_{nn} for the mode I interface and K_{ss} for the mode II interface is fundamental for the obtained results; in fact it affects not only the deformation of the system but also the hysteretic width of loops in stress-strain curves.

As displacements at failure of the interfaces, we adopted the arbitrary high values 10 μm and 3 μm, respectively for the undamageable interfaces and for the damageable interface. These levels of displacement values are never achieved by the finite elements in our simulations, over the course of the stress and strain range seen experimentally, and are hence selected to make sure that the damage occurs only in terms of stiffness degradation and never of complete failure. Specifically, we assumed that the stresses are always transferred through the interfaces. For damageable interfaces, once the damage initiates, the stiffness follows the degradation law: K' = (1 - d) K, where d ϵ [0, 1] is the damageable variable. The total dissipated energy dissipated (per unit of area) through the process of damage of the interface is the area under the traction-separation curve (represented as G_c

in **Figure 2b**). In **Table 1** we schematically summarise the values adopted for the cohesive simulations.

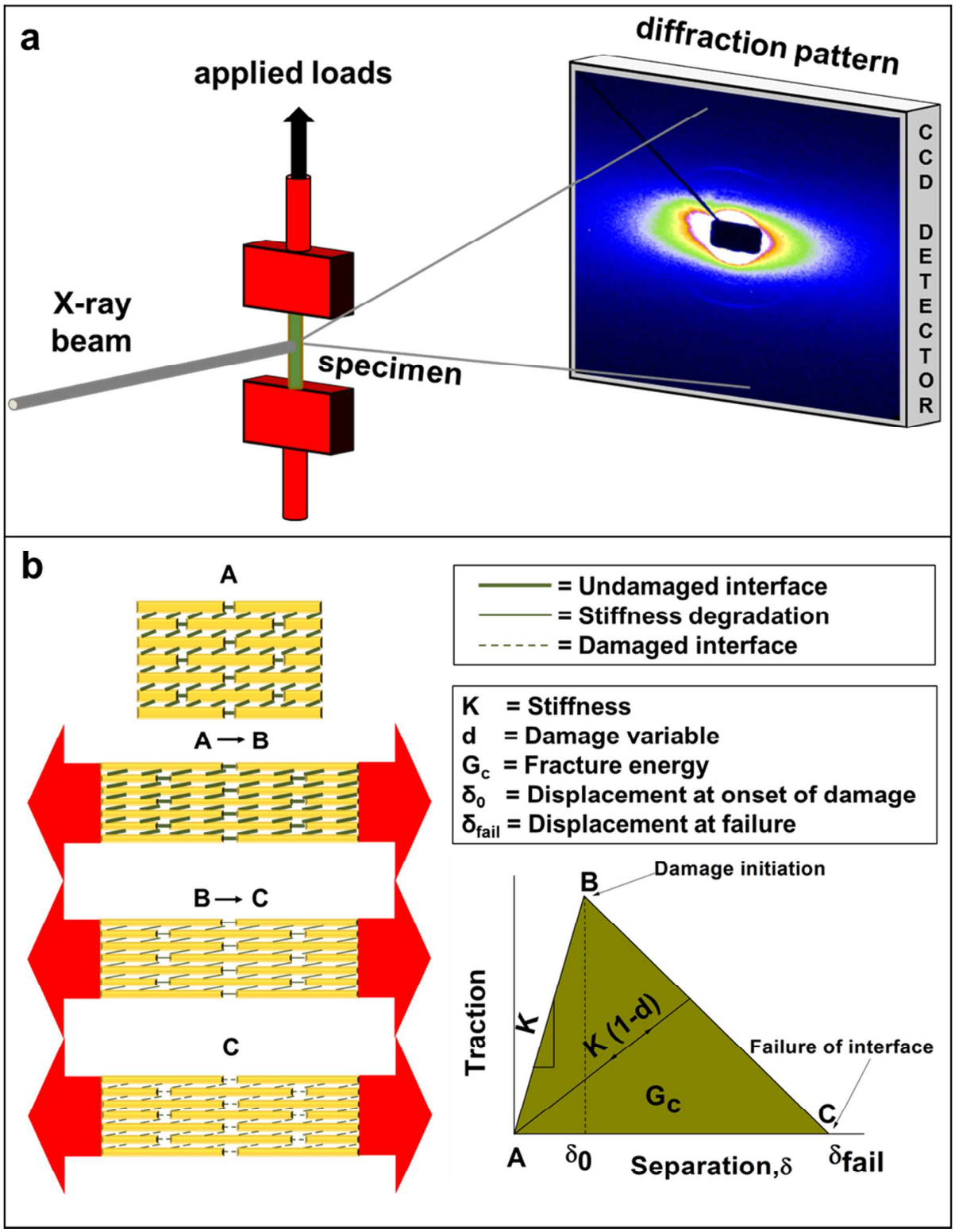

Figure 2 - Experimental and numerical methods: (*a) experimental setup in synchrotron. Mechanical tester design for tensile testing. (b) Staggered fibril structure at the scale of 0.1 - 10 µm with cohesive surface behaviors at the interface. The interfibrillar interface is*

modeled with a cohesive-traction separation law. A-B: linear stiffness; B: onset of damage; B-C: damage evolution curve characterized by the stiffness degradation coefficient (1-d) K; C: failure of interface.

	Mode I interface	**Mode II undamageable interface**	**Mode II damageable interface**
Elastic constant for fracture mode I: **K_{nn} [MPa/μm]**	**100**	100	100
Elastic constant for fracture mode II: **K_{ss} [MPa/μm]**	100	**100**	100
Peak traction for fracture mode I: **t_n^0 [MPa]**	**80**	80	100
Peak traction for fracture mode II: **t_s^0 [MPa]**	80	80	**0.8**
Separation value **δ [μm]**	10	10	**3**

Table 1 – *Input values for cohesive models used in the FE analyses. Bold fonts indicate the parameters that critically affect the simulations.*

The material properties adopted for the fibrils follow a previous model (**Figure 3a**)[20], with the Young's modulus of 15.8 GPa and the yielding of 46 MPa (**Figure 3b**). In other words, the elastoplastic behaviour of a single fibril, and its yield point and stiffness, are taken as a given, and arise from previous experimental work (Gupta et al.[20, 39]). Tensile and cyclic static simulations were performed to study respectively the biphasic fibrillar deformation (section 3.1) and hysteretic loops in stress-strain curves. The applied loads reproduce the values used for experiments by Gupta et al.[20]. Uniaxial traction, along the direction 1 (see **Figure 3c**), was applied to the top end of the finite element models and fixed support to the bottom end, while right and left sides were kept unconstrained. In detail, a traction value of 60 MPa was imposed for the static tests and a sequence of different traction values for the cyclic tests (43 – 0 - 50 – 0 – 56 – 0 – 60 – 0 – 43 MPa). The uniaxial tissue strain was computed as ratio between the displacement of the loaded edge and the initial length, not by averaging the strain field. This is because the average of the strains over the structure does not account for the deformation of the cohesive interfaces. In fact, since cohesive interfaces are essentially springs, small gaps appear between the fibrils (visible, for example, in **Figure 4c**). These gaps are not cracks, but only representative of relative displacements between fibrils.

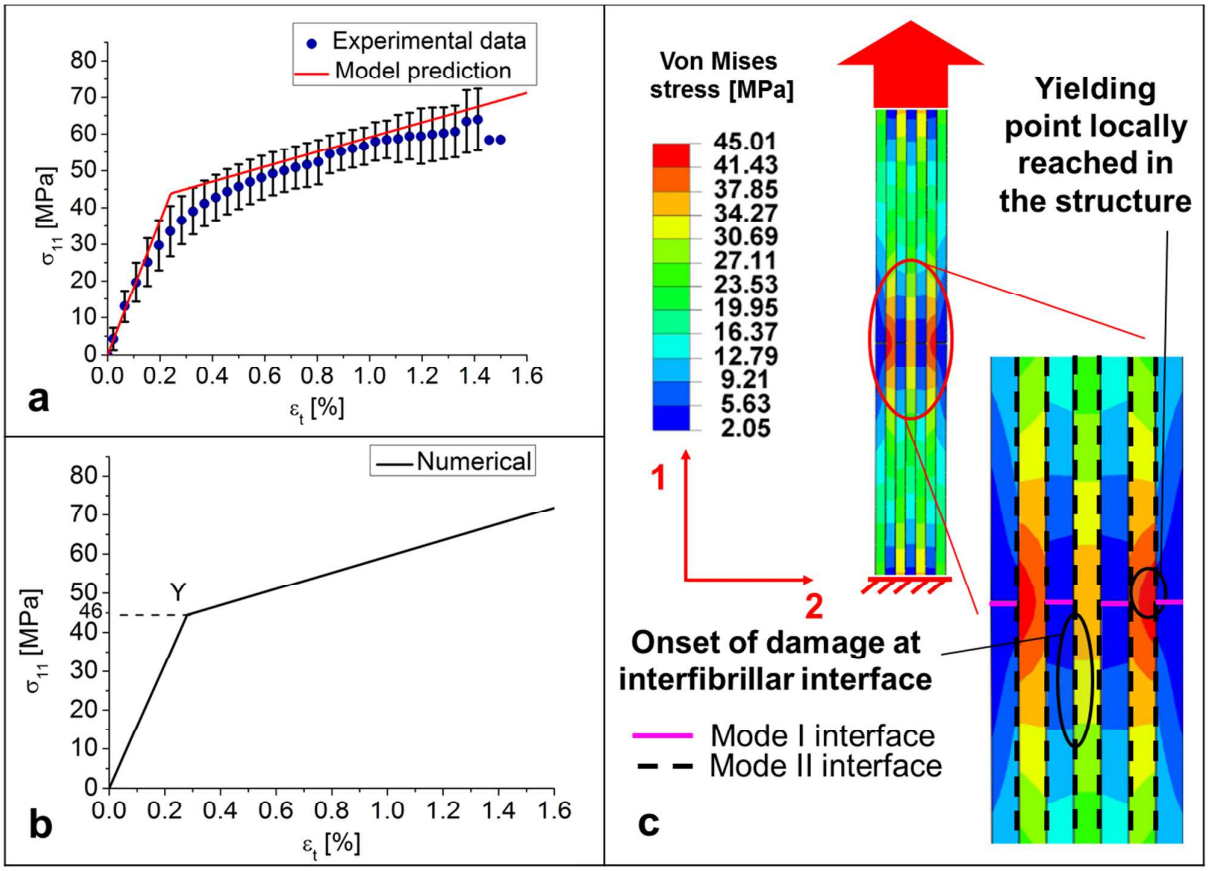

Figure 3 - Experimental and numerical fibril stress-strain curves: *(a) Experimental stress-strain curve for antler bone versus model prediction. Data are averaged from 10 uniaxial stretch-to-failure tests and bars are standard deviations. (b) Material properties input for simulations. (c) Cohesive interface characterization. The interface surrounding the central fibril starts damaging when at least one finite element of the whole structure reaches yielding at 46 MPa (maximum stress criterion).*

3 RESULTS

3.1 Biphasic fibrillar deformations

As stated earlier, a main experimental finding in Gupta et al.[20] was a biphasic fibrillar deformation. Our aim was to understand the role of cohesive interfibrillar surface interfaces in staggered mineralized fibril models, in enabling this behaviour. In this regard the multi-panel **Figure 4** shows an overview comparing strain distributions between experimental data and numerical simulations. These will be explored in detail below.

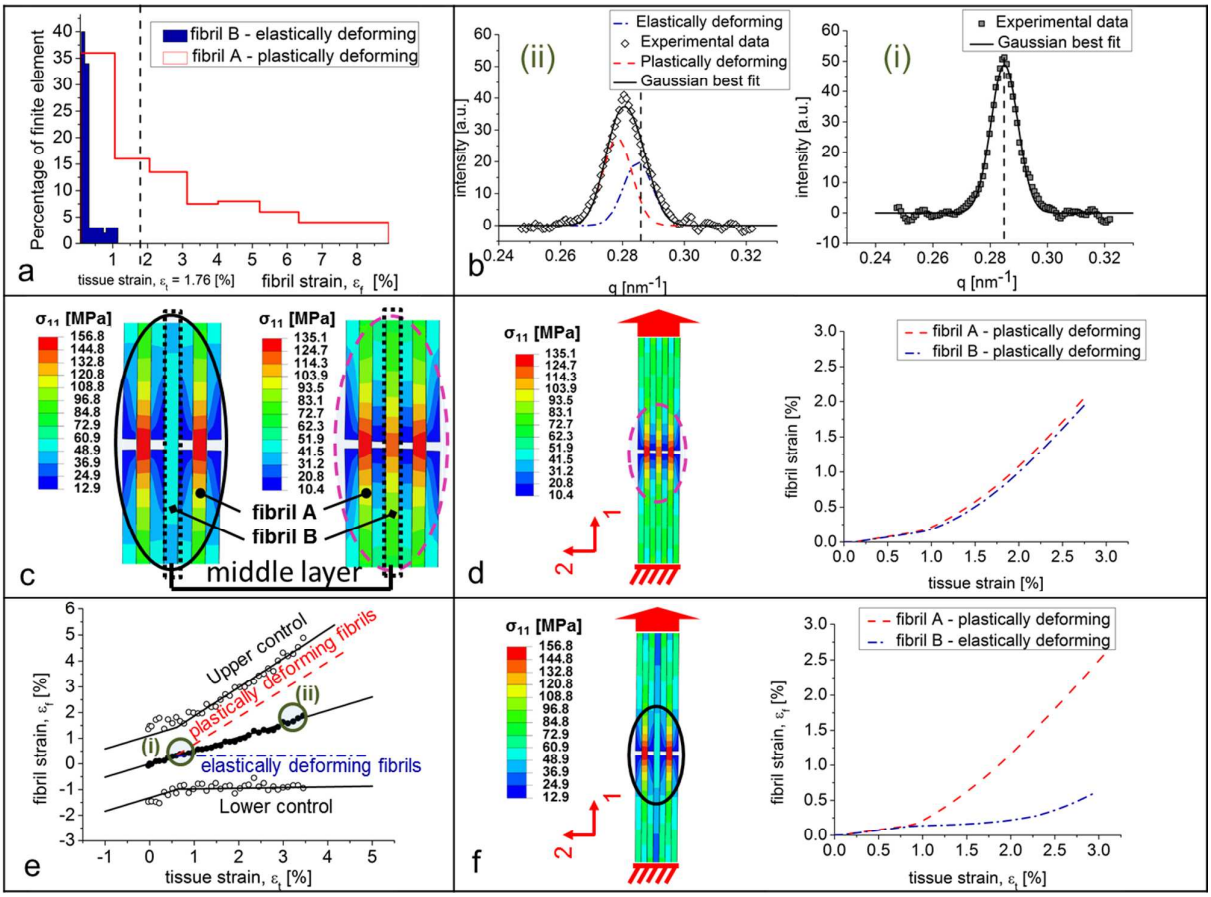

Figure 4 – Experimental and numerical fibrillar deformation mechanisms: *(a) Strain distribution for elastically and plastically deforming fibrils for a tissue strain value of 1.76 %. (b) SAXD intensity plots. (i) Tissue strain at the yield value of 0.6 % (highlighted by a circle and the letter (i) in Figure c). (ii) Tissue strain at the value of 3.2 % (highlighted by a circle and the letter (ii) in Figure c). (c) Stress distributions with and without damageable interfaces. Zoom from Figures d and f. (d) Fibril behaviors in presence of undamageable*

interfaces between fibrils. Fibril b, at the center of the middle layer, deforms plastically. (e) Variation of mean fibril strain (filled circles) and upper and lower control lines plotted against tissue strain. The middle solid line is the linear regression against tissue strain. (f) Fibril behaviors in presence of damageable interface only between the middle layer and the adjacent two layers. Fibril b, at the center of the middle layer, deforms elastically.

For tensile simulations, we firstly adopted a non-damageable law for both the mode I and the mode II interfaces, shown previously in **Figure 3c**. The results of applied uniaxial traction on the fibrils are shown in **Figure 4d**, with relative magnification in **Figure 4c**, with both fibrils A and B plastically deforming, as expected. The maximum longitudinal stress (σ_{11}), reached in central region of the fibrils, is 135 MPa in fibril A and 119 MPa in fibril B, while the averaged stresses are respectively 65 MPa and 63 MPa, beyond the yield point.

Secondly, we found that the introduction of damageable mode II interface around the middle layer produces a differentiation of the fibril behaviors. The damage of the interface around the middle layer partially 'isolates' fibril B, which is then not able to fully contribute to the load absorption. While fibril A remains elastoplastic in its deformation behaviour, the deformation of fibril B never exceeds the elastic range (**Figures 4c - f**). In fact, although the maximum longitudinal stress (σ_{11}), locally measured in a restricted region of fibril B, is 58 MPa (beyond the yield point), its homogenized stress is below the yield point (39 MPa). The corresponding values for fibril A are respectively 157 MPa and 73 MPa. Considering a particular level of macroscopic tissue strain beyond the yield point, such as ε_t = 1.76 % (**Figure 4a**), we find that most of the load (86 %) is carried by fibril A whose finite elements are able to stretch up to eight times more than the finite elements in fibril B. For this tissue strain value, the largest deformation in fibril A is ε_f = 8.9 % whilst in fibril B is ε_f = 1.2 %. In

addition, the average deformation of fibril A is 0.9 % while for the fibril B the equivalent strain is 0.2 % (below the yield point).

In **Figure 4f**, curves show that numerical results are in good agreement with the experimental results shown in **Figure 4e,** where a comparison between experimental results and model predictions, developed by Gupta et al.[20], is presented. In particular, the figure includes the upper and lower control lines ($\varepsilon_{f,\pm 25\%}$), the best fit linear regression against tissue strain (middle solid line), and the model predictions for both the elastically deforming fibril (blue dash-dotted line) and the plastically deforming fibrils (red dashed line). In **Figures 4f - e**, the elastic and plastic patterns are clearly observable, as also demonstrated by the experimental results in **Figure 4b**, where the SAXD intensity plot (**Figure 4b (i)**) shows that all the fibrils are elastic at the yielding point (tissue strain = 0.6 %), while for a tissue strain of 3.2 % (**Figure 4b (ii)**) the coexistence of plastic and elastic fibrils occurs, with 58% of fibrils at ε_f = 2.95 % (plastic strain) whilst the remainder fraction at ε_f = 0.53% (elastic strain).

3.2 The role of mode II interfaces in cyclic loading

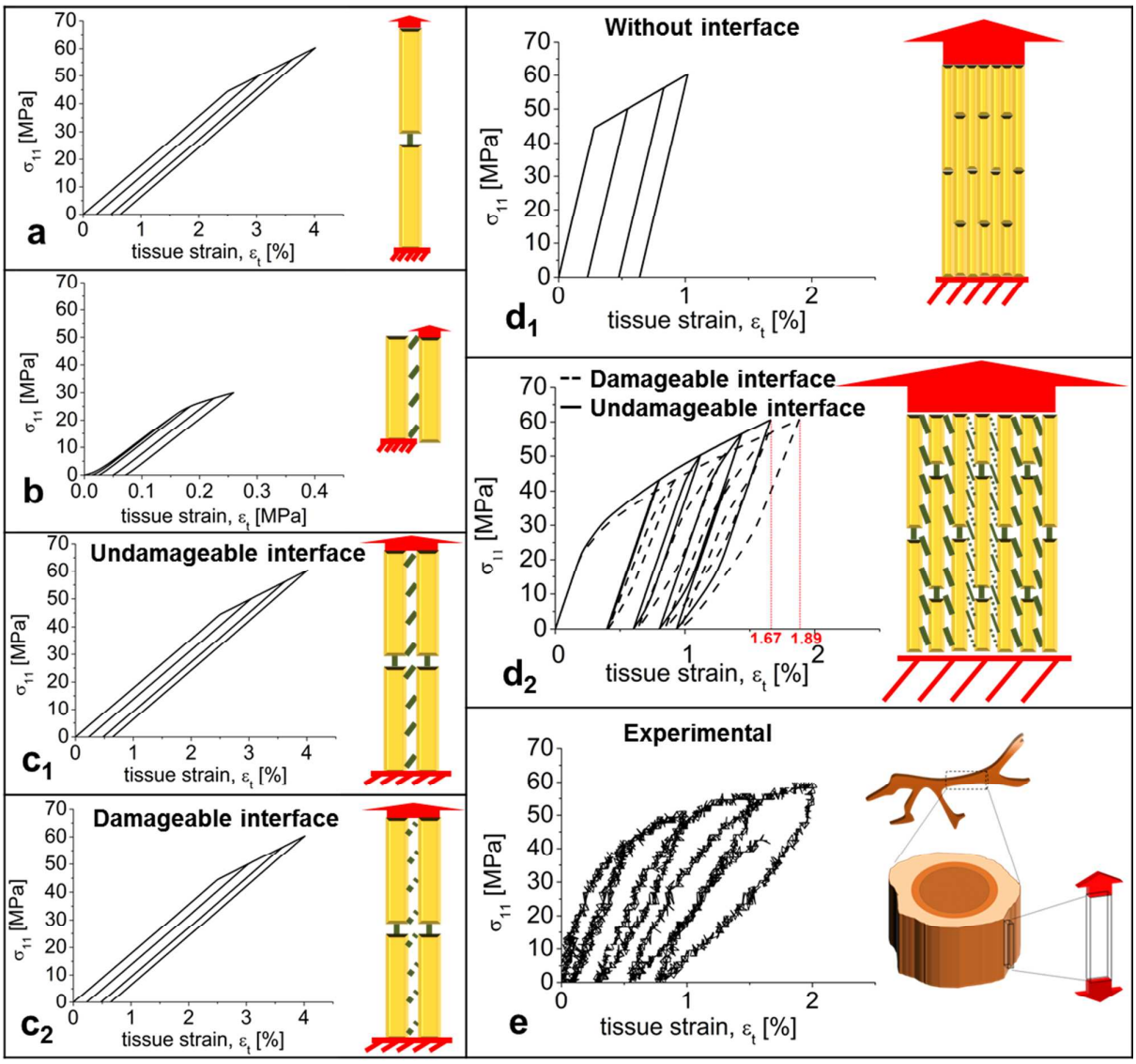

Figure 5 - Cyclic loading in different fibrillar geometries: *Comparisons between numerical (figures a, b, c_1, c_2, d_1, d_2) and experimental results (figure e). (a) Two fibrils model with 'mode I' non damageable interface. (b) Two fibrils model with 'mode II' non damageable interface. (c_1) Four fibrils model with 'mode I' and 'mode II' non damageable interfaces, in aligned configuration. (c_2) Four fibrils model with 'mode I' non damageable interface and 'mode II' damageable interface, in aligned configuration. (d_1) Seven layers model without interfaces, in staggered configuration. (d_2) Comparison between two seven*

layers models in staggered configuration: damageable mode II interfaces at the middle layer versus undamageable ones. (e) Experimental results for cyclic loading on bone.

A second main finding in Gupta et al.[20] was the existence of hysteresis at the fibrillar level. The elasto-plastic behaviors of a set of different models under cyclic loading were simulated to discover the combined effects of fibril lateral arrangement and architecture, coupled with the interface types described in the previous subsection. We found that the experimentally observed hysteresis in the cyclic loading curves occurs when staggered fibril arrangement coupled with mode I and mode II cohesive surface interfaces are introduced in cyclic simulations. In fact, the presence of only mode I or mode II interfaces for, respectively, a system of two aligned or two-column fibrils is clearly not responsible for hysteresis (**Figures 5a - b**). These effects do not arise from the limited number of fibrils considered: an increase in number of fibrils from two to four, in a condition of non-overlap, results in no hysteresis with both damageable and undamageable mode II interfaces (**Figure 5c1 – c2**). As fibrils do not transmit load through shearing in the configurations shown in **Figures 5c1 - c_2**, no difference between damageable and undamageable mode II interface is observed. From our set of simulations, we observed that only the concurrence of staggered fibril arrangement and cohesive surface interface (not necessary damageable) leads to hysteresis in loading/unloading stress strain curves (**Figure 5d2**). It can be seen from **Figure 5d1** that staggered but perfectly bonded fibrils (no cohesive interface) do not exhibit hysteresis and loading/unloading patterns perfectly overlap. The introduction of damageable mode II interfaces makes the structure more deformable. Indeed, as fibrils, in staggered configuration, transmit loading through shearing, damageable and then weaker mode II interfaces allow the whole structure to deform up to 1.89 %, while in a condition of non-damageable interfaces the tissue strain reaches the value of 1.67 % (**Figure 5d2**) at the same stress level of 60 MPa.

Numerical results for the cyclic loading curves are in very good agreement with experimental data (comparisons in **Figures 5d2** and **5e**). Maximum tissue strains, in both cases, are about 1.9 % and furthermore, the structural yielding points occur at tissue strain ≈ 0.22 % and axial stress ≈ 25 MPa, earlier than the corresponding prediction in the material law[20] used for simulations.

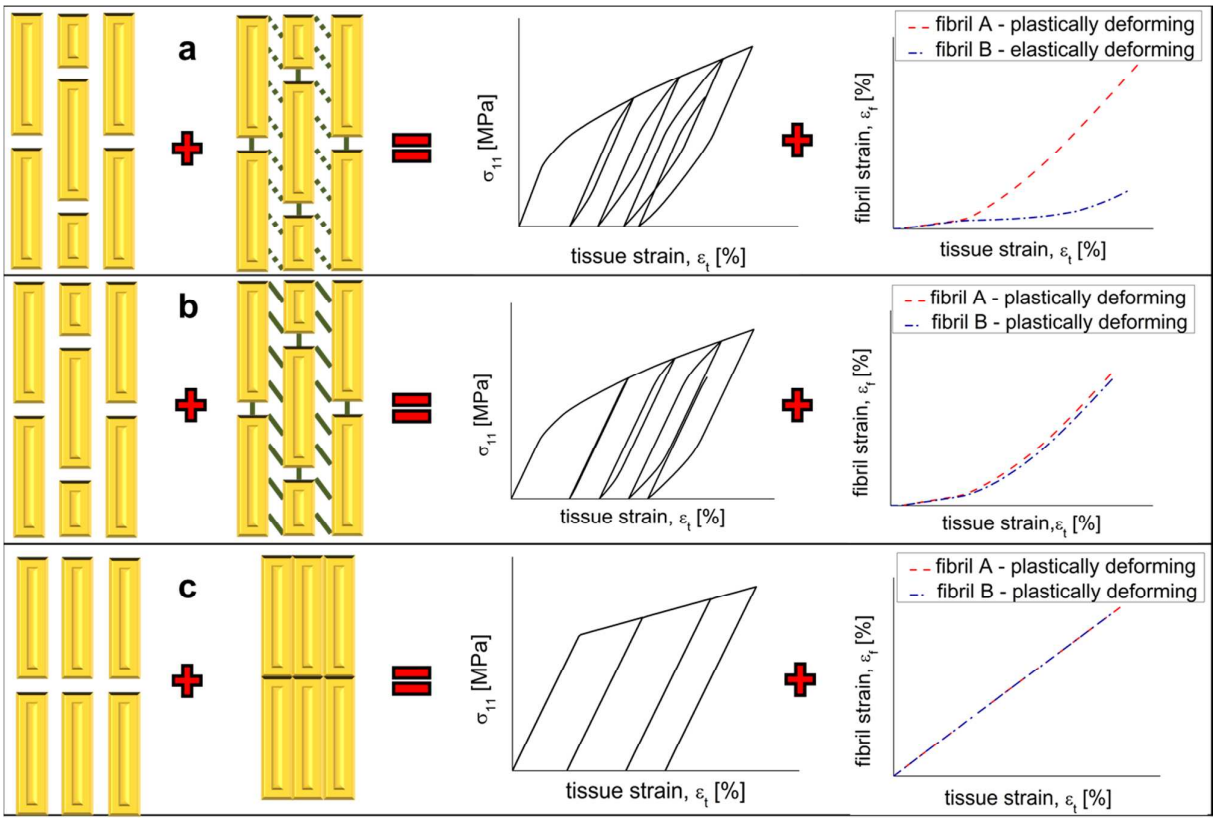

Figure 6 - Summary of main results: *(a) Staggered fibrillar configuration and damageable mode II interface are responsible for hysteretic stress strain curve and heterogeneous fibrillar deformation. (b) The inclusion of staggered configuration and undamageable interface leads to hysteresis and homogeneous fibril deformation. (c) Aligned fibrillar configuration and no interface lead to no hysteresis and homogeneous fibril deformation.*

This paper shows how combination of finite elements simulations at fibrillar level, combined with experimentally derived information on ultrastructural plasticity of the fibril, enables the development of a model for the mechanical behaviors of antler bone under cyclic loading conditions which can explain both the energy dissipation (via hysteresis) as well as the concurrent heterogeneous pattern at the nanoscale. In addition, as shown in **Figure 6**, our parametric simulations allow us to conclude that the combination of:

a. staggered fibrillar configuration and damageable mode II interface leads to hysteresis and fibrillar heterogeneity;
b. staggered fibrillar configuration and undamageable mode II interface leads to hysteresis and fibrillar homogeneity;
c. aligned fibrillar configuration and perfectly bonded boundary conditions (without cohesive behaviors) at the interfaces leads to no hysteresis and fibrillar homogeneity.

4 DISCUSSION AND CONCLUSION

Elastic deformation in bone at the nanoscale has been extensively studied[4, 32, 40-42] via multiscale fibre composite models that often treat bone material as a two-scale hierarchical composite; mineralized fibrils are arranged in a staggered manner, and fibrils themselves consist of mineral platelets staggered in a collagen matrix phase. Such models are usually validated by comparing the tissue-level modulus predictions to experimentally determined stiffness, though in an ideal scenario predictions of deformation and stress at multiple levels would be calculated and compared to experiment.

In the area of structural models for inelastic and damage accumulation in bone, there are no modeling attempts for the structural response of the nanoscale bone material under

cyclic loading. To fill this gap, here we proposed a model based on surface cohesive behaviors. Our main assumptions are to neglect the material properties of the interfibrillar matrix and to consider the fibrils linked by cohesive surfaces whose damage process occurs in terms of stiffness degradation. Previously, cohesive behaviours were used for studying the damage mechanisms of bone at different scales[43-47]. Our approach, on the contrary, is based on cohesive stiffness representative of interfaces with negligible small thicknesses. The main difference between the two approaches is that in surface-based laws the damage evolution describes the degradation of the cohesive stiffness whereas in the continuum-based approach[43-47] the damage concerns the degradation of the material stiffness. The continuum model, called also cohesive zone model, can be used to analyse both interface and bulk fracture. For example, Hamed and Jasiuk[43] created a multiscale model for studying the mechanisms of damage in bone and used the cohesive zone for modelling the fracture of the interface between collagen and hydroxyapatite platelets but also the fracture inside the fibrillar components. They found that the mesh size of cohesive elements had a significant effect on the strength of the mineralized fibrils. A recent study[46] investigated the evolution of damage in staggered array of mineralised collagen fibrils (MCF) embedded in extrafibrillar protein matrix modelled by continuum cohesive finite elements. The authors found that the failure mechanisms of the extrafibrillar matrix play a dominant role on the energy dissipation capacity of the system. Lin et al.[47] recently provided evidence as to the importance of the extrafibrillar matrix, considered as composite of hydroxyapatite crystals embedded in an interface modelled by cohesive finite elements, in the pre-yield deformation and failure mode of bone. They found that a tough interface provokes ductile deformation of matrix, as in the case of wet bone, whereas a brittle interface causes brittle deformation, as in dry bone.

Hysteresis, at higher scales in bone, has been found in experiments, but relatively few bone-specific models exist. Ascenzi et al.[48] tested single osteons and found hysteresis loops under tension. They discovered that the collagen orientation is the main factor to determine the features of hysteresis loops. In both our experimental work and in other references such as Ascenzi et al.[48], the width of hysteretic loops tends to increase as the applied stress increases. In terms of modelling of the hysteresis loop width, the work of A. G. Evans and co-workers, who carried out modelling and numerical analysis of ceramic matrix composite deformation[49], is relevant, although their model is applied to a different class of synthetic materials. They derived expressions for which the maximum hysteresis loop width depends on the Young's modulus of both, the fibrils and the matrix, the fibril radius and the fibril volume fraction, but also on the stress conditions, such as the maximum stress reached in the system. At lower scales an analytical model explained the inelastic response of bone[50], indicating stress/strain hysteresis in loading/unloading tests. The authors found the shear yielding of the interface between collagen fibrils and mineral platelets to be the cause of irreversible slip and then of hysteresis. Hysteresis, in our staggered fibrillar models, is due to the presence of cohesive surface interfaces and in detail, to zones of stress concentration. In fact, we found that, once stretched or released (null surface traction applied to the structure) finite elements of the horizontally adjacent fibrils (fibrils on the same layer) are under-loaded, while finite elements of the underlying fibrils are over-loaded (**Figure 4c**). This mechanism results in a certain delay of the structure, manifesting as hysteretic loops, necessary to reach the traction value imposed at following loading or unloading steps.

Our second finding regards heterogeneous fibrillar deformation caused by partially damageable interfaces. Heterogeneity in the behaviors of mineralized tissue was detected as a mechanism contributing to energy dissipation [19, 22]. Mechanical properties of

individual mineralized collagen have been only recently analyzed thanks to the development of innovative experimental techniques. While the fibrillar structure of collagenous tissues was explored extensively during the last decades (for a review see [39]), only more recently have their mechanical properties been determined experimentally[18, 51]. Heterogeneity in fibrillar deformation were found in antler cortical tissue by Krauss et al.[34] by using a time-resolved synchrotron small angle X-ray diffraction technique, coupled with tensile testing. They found that heterogeneity in fibrillar deformations starts after the macroscopic yielding. Hang and Barber[18] performed tensile testing on individual fibrils from antler using atomic force microscopy and scanning electron microscopy. They found heterogeneous deformations in fibrils showing either yield or strain hardening. The structural mechanism for interfacial failure between fibrils may involve the breakage of sacrificial bonds in the noncollageneous proteins found in the interfibrillar matrix[22]. These weak calcium mediated bonds within and between proteins such as osteopontin or osteonectin have been proposed to play a significant role in bone toughness[52-53] Recently, Poundarik et al.[21] proposed a mechanism of clusters of extrafibrillar mineral held together by non-collagenous protein glue. Under deformation, this model generates an inhomogeneous strain and stress pattern at the fibrillar level. While we found, instead, that damageable mode II interfaces are responsible for heterogeneous strain fields, the structural origin of such damage may involve mechanisms as proposed by Poundarik et al.[21] . In detail, fibrils surrounded by damageable interfaces behave elastically while other fibrils reach higher stress values after yielding (**Figure 7a** in Appendix 1). At lower scales, Buehler[25] found the existence of a range of adhesive energy values between molecule (0.01 – 1 J/m^2) which optimizes the toughening mechanisms. Following this concept of optimization, a possible application of our model may be a quantitative and parametric approach to evaluate the types of mechanical behaviors of interfaces which lead to optimized toughness. It must be remarked that in our models, we consider damage only as

stiffness degradation of cohesive surfaces and not as failure and that we use a 2D model. In terms of multiscale modelling of toughness, the current model will allow one to homogenize the properties at the fibrillar scale and these homogenized properties could be inserted into a larger-scale 3D model for the study of crack propagation and damage in real antler bone.

In conclusion, by constructing a finite element model for the inelastic cyclic loading response of mineralized collagen fibrils in antler, we show that the hysteresis observed is due to interfibrillar staggering leading to inhomogeneous stress fields along the fibril and localized intrafibrillar plasticity, while the inhomogeneous deformation arises from the weak interfaces between fibrils, potentially mediated by sacrificial bonds in the noncollageneous proteins between fibrils.

5 ACKNOWLEDGMENTS

HSG thanks Peter Fratzl and Stefanie Krauss (Max Planck Institute of Colloids and Interfaces, Potsdam, Germany), Dr. Sergio Funari (HASYLAB-DESY, beamline A2) and Prof. John Currey (University of York) for very pleasant scientific collaboration on earlier work on antler bone[20, 34]. EB is supported by the Queen Mary University of London Start-up grant for new academics. NMP is supported by the European Research Council (ERC StG Ideas 2011 BIHSNAM n. 279985, ERC PoC 2015 SILKENE nr. 693670), by the European Commission under the Graphene Flagship (WP14 Polymer Nanocomposites, n. 696656).

6 REFERENCES

1. Meyers, M. A.; Chen, P.-Y.; Lin, A. Y.-M.; Seki, Y., Biological materials: structure and mechanical properties. *Progress in Materials Science* **2008,** *53* (1), 1-206.
2. Fratzl, P.; Weinkamer, R., Nature's hierarchical materials. *Progress in Materials Science* **2007,** *52* (8), 1263-1334.
3. Buehler, M. J., Nano-and micromechanical properties of hierarchical biological materials and tissues. *Journal of Materials Science* **2007,** *42* (21), 8765-8770.
4. Ji, B.; Gao, H., Mechanical properties of nanostructure of biological materials. *Journal of the Mechanics and Physics of Solids* **2004,** *52* (9), 1963-1990.
5. Weiner, S.; Wagner, H. D., The material bone: structure-mechanical function relations. *Annual Review of Materials Science* **1998,** *28* (1), 271-298.
6. Bonderer, L. J.; Studart, A. R.; Gauckler, L. J., Bioinspired design and assembly of platelet reinforced polymer films. *Science* **2008,** *319* (5866), 1069-1073.
7. Pugno, N. M., Mimicking nacre with super-nanotubes for producing optimized super-composites. *Nanotechnology* **2006,** *17* (21), 5480.
8. Bosia, F.; Buehler, M. J.; Pugno, N. M., Hierarchical simulations for the design of supertough nanofibers inspired by spider silk. *Physical Review E* **2010,** *82* (5), 056103.
9. Bosia, F.; Abdalrahman, T.; Pugno, N. M., Self-healing of hierarchical materials. *Langmuir* **2014,** *30* (4), 1123-1133.
10. Bosia, F.; Abdalrahman, T.; Pugno, N. M., Investigating the role of hierarchy on the strength of composite materials: evidence of a crucial synergy between hierarchy and material mixing. *Nanoscale* **2012,** *4* (4), 1200-1207.
11. Wang, Y.; Azaïs, T.; Robin, M.; Vallée, A.; Catania, C.; Legriel, P.; Pehau-Arnaudet, G.; Babonneau, F.; Giraud-Guille, M.-M.; Nassif, N., The predominant role of collagen in the nucleation, growth, structure and orientation of bone apatite. *Nature materials* **2012,** *11* (8), 724-733.
12. Dimas, L. S.; Bratzel, G. H.; Eylon, I.; Buehler, M. J., Tough composites inspired by mineralized natural materials: computation, 3D printing, and testing. *Advanced Functional Materials* **2013,** *23* (36), 4629-4638.
13. Compton, B. G.; Lewis, J. A., 3D-printing of lightweight cellular composites. *Advanced Materials* **2014,** *26* (34), 5930-5935.
14. Koester, K. J.; Ager, J.; Ritchie, R., The true toughness of human cortical bone measured with realistically short cracks. *Nature materials* **2008,** *7* (8), 672-677.
15. Fleck, C.; Eifler, D., Deformation behaviour and damage accumulation of cortical bone specimens from the equine tibia under cyclic loading. *Journal of biomechanics* **2003,** *36* (2), 179-189.
16. Nalla, R. K.; Kinney, J. H.; Ritchie, R. O., Mechanistic fracture criteria for the failure of human cortical bone. *Nature materials* **2003,** *2* (3), 164-168.
17. Vashishth, D.; Behiri, J.; Bonfield, W., Crack growth resistance in cortical bone: concept of microcrack toughening. *Journal of biomechanics* **1997,** *30* (8), 763-769.
18. Hang, F.; Barber, A. H., Nano-mechanical properties of individual mineralized collagen fibrils from bone tissue. *Journal of the Royal Society Interface* **2011,** *8* (57), 500-505.
19. Tai, K.; Dao, M.; Suresh, S.; Palazoglu, A.; Ortiz, C., Nanoscale heterogeneity promotes energy dissipation in bone. *Nature materials* **2007,** *6* (6), 454-462.
20. Gupta, H.; Krauss, S.; Kerschnitzki, M.; Karunaratne, A.; Dunlop, J.; Barber, A.; Boesecke, P.; Funari, S.; Fratzl, P., Intrafibrillar plasticity through mineral/collagen sliding is the dominant

mechanism for the extreme toughness of antler bone. *Journal of the mechanical behavior of biomedical materials* **2013,** *28*, 366-382.
21. Poundarik, A. A.; Diab, T.; Sroga, G. E.; Ural, A.; Boskey, A. L.; Gundberg, C. M.; Vashishth, D., Dilatational band formation in bone. *Proceedings of the National Academy of Sciences* **2012,** *109* (47), 19178-19183.
22. Fantner, G. E.; Hassenkam, T.; Kindt, J. H.; Weaver, J. C.; Birkedal, H.; Pechenik, L.; Cutroni, J. A.; Cidade, G. A.; Stucky, G. D.; Morse, D. E., Sacrificial bonds and hidden length dissipate energy as mineralized fibrils separate during bone fracture. *Nature materials* **2005,** *4* (8), 612-616.
23. Launey, M. E.; Buehler, M. J.; Ritchie, R. O., On the mechanistic origins of toughness in bone. *Annual review of materials research* **2010,** *40*, 25-53.
24. Tai, K.; Ulm, F.-J.; Ortiz, C., Nanogranular origins of the strength of bone. *Nano letters* **2006,** *6* (11), 2520-2525.
25. Buehler, M. J., Molecular nanomechanics of nascent bone: fibrillar toughening by mineralization. *Nanotechnology* **2007,** *18* (29), 295102.
26. Gupta, H. S.; Wagermaier, W.; Zickler, G. A.; Raz-Ben Aroush, D.; Funari, S. S.; Roschger, P.; Wagner, H. D.; Fratzl, P., Nanoscale deformation mechanisms in bone. *Nano Letters* **2005,** *5* (10), 2108-2111.
27. Zioupos, P.; Currey, J., The extent of microcracking and the morphology of microcracks in damaged bone. *Journal of Materials Science* **1994,** *29* (4), 978-986.
28. Schwiedrzik, J.; Raghavan, R.; Bürki, A.; LeNader, V.; Wolfram, U.; Michler, J.; Zysset, P., In situ micropillar compression reveals superior strength and ductility but an absence of damage in lamellar bone. *Nature materials* **2014,** *13* (7), 740-747.
29. Barthelat, F.; Rabiei, R., Toughness amplification in natural composites. *Journal of the Mechanics and Physics of Solids* **2011,** *59* (4), 829-840.
30. Buehler, M. J.; Yung, Y. C., Deformation and failure of protein materials in physiologically extreme conditions and disease. *Nature materials* **2009,** *8* (3), 175-188.
31. Bar-On, B.; Wagner, H. D., Mechanical model for staggered bio-structure. *Journal of the Mechanics and Physics of Solids* **2011,** *59* (9), 1685-1701.
32. Bar-On, B.; Wagner, H. D., Structural motifs and elastic properties of hierarchical biological tissues–A review. *Journal of structural biology* **2013,** *183* (2), 149-164.
33. Xia, W.; Ruiz, L.; Pugno, N. M.; Keten, S., Critical length scales and strain localization govern the mechanical performance of multi-layer graphene assemblies. *Nanoscale* **2016,** *8* (12), 6456-6462.
34. Krauss, S.; Fratzl, P.; Seto, J.; Currey, J. D.; Estevez, J. A.; Funari, S. S.; Gupta, H. S., Inhomogeneous fibril stretching in antler starts after macroscopic yielding: Indication for a nanoscale toughening mechanism. *Bone* **2009,** *44* (6), 1105-1110.
35. Gupta, H. S.; Seto, J.; Wagermaier, W.; Zaslansky, P.; Boesecke, P.; Fratzl, P., Cooperative deformation of mineral and collagen in bone at the nanoscale. *Proceedings of the National Academy of Sciences* **2006,** *103* (47), 17741-17746.
36. Dong, X. N.; Almer, J. D.; Wang, X., Post-yield nanomechanics of human cortical bone in compression using synchrotron X-ray scattering techniques. *Journal of biomechanics* **2011,** *44* (4), 676-682.
37. Zimmermann, E. A.; Schaible, E.; Bale, H.; Barth, H. D.; Tang, S. Y.; Reichert, P.; Busse, B.; Alliston, T.; Ager, J. W.; Ritchie, R. O., Age-related changes in the plasticity and toughness of human cortical bone at multiple length scales. *Proceedings of the National Academy of Sciences* **2011,** *108* (35), 14416-14421.
38. Xu, X.-P.; Needleman, A., Numerical simulations of fast crack growth in brittle solids. *Journal of the Mechanics and Physics of Solids* **1994,** *42* (9), 1397-1434.

39. Wess, T.; Cairns, D., Nanoarchitectures of the animal extracellular matrix: opportunities for synchrotron radiation studies on collagen and fibrillin. *Journal of synchrotron radiation* **2005,** *12* (6), 751-757.
40. Hamed, E.; Lee, Y.; Jasiuk, I., Multiscale modeling of elastic properties of cortical bone. *Acta Mechanica* **2010,** *213* (1-2), 131-154.
41. Nikolov, S.; Raabe, D., Hierarchical modeling of the elastic properties of bone at submicron scales: the role of extrafibrillar mineralization. *Biophysical journal* **2008,** *94* (11), 4220-4232.
42. Jäger, I.; Fratzl, P., Mineralized collagen fibrils: a mechanical model with a staggered arrangement of mineral particles. *Biophysical journal* **2000,** *79* (4), 1737-1746.
43. Hamed, E.; Jasiuk, I., Multiscale damage and strength of lamellar bone modeled by cohesive finite elements. *journal of the mechanical behavior of biomedical materials* **2013,** *28*, 94-110.
44. Ural, A., Prediction of Colles' fracture load in human radius using cohesive finite element modeling. *Journal of biomechanics* **2009,** *42* (1), 22-28.
45. Mischinski, S.; Ural, A., Finite element modeling of microcrack growth in cortical bone. *Journal of Applied Mechanics* **2011,** *78* (4), 041016.
46. Lai, Z. B.; Yan, C., Mechanical behaviour of staggered array of mineralised collagen fibrils in protein matrix: Effects of fibril dimensions and failure energy in protein matrix. *Journal of the Mechanical Behavior of Biomedical Materials* **2017,** *65*, 236-247.
47. Lin, L.; Samuel, J.; Zeng, X.; Wang, X., Contribution of extrafibrillar matrix to the mechanical behavior of bone using a novel cohesive finite element model. *Journal of the Mechanical Behavior of Biomedical Materials* **2017,** *65*, 224-235.
48. Ascenzi, A.; Benvenuti, A.; Mango, F.; Simili, R., Mechanical hysteresis loops from single osteons: technical devices and preliminary results. *Journal of biomechanics* **1985,** *18* (5), 391-398.
49. Vagaggini, E.; Domergue, J. M.; Evans, A. G., Relationships between hysteresis measurements and the constituent properties of ceramic matrix composites: I, theory. *Journal of the American Ceramic Society* **1995,** *78* (10), 2709-2720.
50. Mercer, C.; He, M.; Wang, R.; Evans, A., Mechanisms governing the inelastic deformation of cortical bone and application to trabecular bone. *Acta Biomaterialia* **2006,** *2* (1), 59-68.
51. Shen, Z. L.; Dodge, M. R.; Kahn, H.; Ballarini, R.; Eppell, S. J., Stress-strain experiments on individual collagen fibrils. *Biophysical Journal* **2008,** *95* (8), 3956-3963.
52. Thurner, P. J.; Chen, C. G.; Ionova-Martin, S.; Sun, L.; Harman, A.; Porter, A.; Ager, J. W.; Ritchie, R. O.; Alliston, T., Osteopontin deficiency increases bone fragility but preserves bone mass. *Bone* **2010,** *46* (6), 1564-1573.
53. Gupta, H. S.; Fratzl, P.; Kerschnitzki, M.; Benecke, G.; Wagermaier, W.; Kirchner, H. O., Evidence for an elementary process in bone plasticity with an activation enthalpy of 1 eV. *Journal of the Royal Society Interface* **2007,** *4* (13), 277-282.

For Table of Contents Use Only

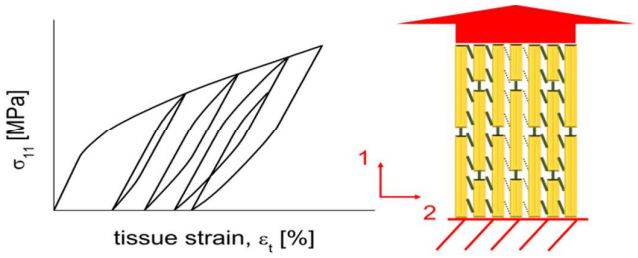

Staggered fibrils and damageable interfaces lead concurrently and independently to hysteretic energy absorption and inhomogeneous strain fields in cyclically loaded antler bone

P. De Falco, E. Barbieri, N. Pugno and H. S. Gupta